Novel, simple, and environmentally safe method for wastewater pollutant removal

Luis Duque [a], Lucia Gutiérrez [b], Nieves Menéndez [a], Pilar Herrasti [a], Eva Mazario [a],[*]

[a] *Departamento de Química Física Aplicada, Facultad de Ciencias, Universidad Autónoma de Madrid, 28049 Madrid, Spain*
[b] *Departamento de Química Analítica, Instituto de Nanociencia y Materiales de Aragón (INMA) CSIC-Universidad de Zaragoza, and CIBER-BBN, 50018 Zaragoza, Spain*
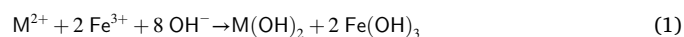
ARTICLE INFO

ABSTRACT

In this work, a new methodology has been developed for the elimination of cobalt, nickel and a mixture of both metals from synthetic wastewater in a continuous way. This methodology consists of the electrochemical formation of ferrites of these metals through the oxidation of iron sheets and the reduction of water. Two critical process parameters, current densities and initial pollutant concentration, were analysed. An initial batch prototype resulted in efficiencies on the order of 98% under conditions of applied densities of 50 mA/cm^2 and concentrations of both metals of until 100 ppm of the ions. The obtained particles have been characterized by X-ray diffraction to determine the formation of ferrites without the appearance of secondary phases. The formed particle sizes are approximately 30 nm, with hemispherical or flower-like shapes. A flow system prototype was designed for the recirculation of the solution with 100 ppm of both contaminating metals, obtaining approximately 90% recovery with an easy magnetic harvesting.

1. Introduction

Heavy metals are a serious problem when dissolved in wastewater and have been the subject of research for decades. Cobalt and nickel in water are usually at low concentrations in ranges of 0.1–5 μg/L and 5–10 μg/L, respectively. However, the concentration can be hundreds or thousands of times higher in areas with minerals or near mines or smelters. To reduce the toxicity associated with such metals, it is desirable to treat industrial effluents to decrease Co(II) and Ni(II) concentrations and decrease them to within permissible limits before being discharged into water bodies. There are many techniques to eliminate or reduce the amount of these metals in water. Chemical precipitation [1], ion exchange [2,3], and adsorption [4–7] are the most commonly used techniques in practical applications for wastewater treatment. One of the chemical methods used is the precipitation of ferrites of these metals [8,9]. The procedure is simple and based on the addition of a Fe^{3+} salt and basic medium to water contaminated with metal ions, allowing the formation of metal ferrite. The reactions that occur are shown in Eqs. (1) and (2):

$$M^{2+} + 2\,Fe^{3+} + 8\,OH^- \rightarrow M(OH)_2 + 2\,Fe(OH)_3 \tag{1}$$

$$M(OH)_2 + 2\,Fe(OH)_3 + Aeration \rightarrow MFe_2O_4 + 4\,H_2O \tag{2}$$

In general, this methodology has been utilized for high concentrations of metal ions. As a result, the ferrites produced by this methodology contain impurities, and there is no control of the obtained material properties.

A similar process can be produced using an electrochemical methodology. C. Huang et al. [10] explored this process to remove Co^{2+} ions from simulated liquid radioactive waste in a nuclear power plant. The method consisted of the oxidation of an iron sheet producing Fe^{3+} ions in the medium and a cathode of iron where the generation of OH$^-$ was produced by water reduction. The overall reaction is essentially the same as in the previous method, but the production of Fe^{3+} and OH$^-$ ions is controlled by the current applied to the electrodes. In addition to the current, the electrochemical method makes it possible to eliminate smaller amounts of ions from the medium, and it is possible to generate ferrites with tunable properties. Metal extraction by electrochemical method is considered a green and safe production strategy to reduce the environmental charge compared to traditional methods [11].

Ferrites find applications in many fields. They are used in biomedicine in magnetic resonance imaging [12], drug delivery [13], hyperthermia [14], or sensors [15,16]. However, their applications in wastewater treatment, can be extended to, photodegradation and heterogeneous fenton-like degradation of dyes, pesticides and

---

* Corresponding author.
E-mail address: eva.mazario@uam.es (E. Mazario).

pharmaceuticals [17,18], adsorption removal of inorganic contaminant, such as As, Cd, Co, Cr, Pb, UO_2^{2+} among others [19–21] and pathogen disinfection [22,23]. The properties of ferrites depend on their composition, cation substitution, preparation technique, and cation distribution in the spinel structure [24,25]. In general, methods such as coprecipitation, hydrothermal methods, sol-gel, etc. have been employed to synthesize ferrites of desired composition and structure. The methodology used here has two advantages: contamination elimination from the medium and ferrites production of different compositions and morphologies, and, therefore, different properties.

In this work, we explored the formation of nickel, cobalt, and nickel-cobalt ferrites by in situ electrochemical synthesis employing different amounts of pollutants and analysing the amount of metal eliminated from the media. In addition, the ferrites obtained have been structurally and magnetically characterized using different techniques. To scale up this methodology, a flow cell was used for the elimination of the metal and formed ferrites [26].

2. Experimental

2.1. Materials

Cobalt chloride ($CoCl_2 \cdot 6H_2O$) and nickel chloride ($NiCl_2 \cdot 6H_2O$), both with purity $\geq$99.5%, were supplied by Sigma-Aldrich Chemical Co (Germany). Sodium chloride (NaCl, $\geq$ 99.5%) was purchased from Merck KGaA (Germany). The iron sheets (purity 99.9%) used as electrodes in the batch, and the low carbon still sheets (99.8% wt iron purity) used as electrodes in the flow reactor were supplied by Goodfellow Inc. (United Kingdom).

2.2. Experimental procedures

2.2.1. Batch pollutant removal

Simulated wastewater solutions with cobalt and nickel (II) ions at different concentrations were prepared by dilution of a 1000 ppm concentrated stock solution. A supporting electrolyte of 40 mM NaCl was used to increase the ionic strength of the solution. A cylindrical cathode of iron 120 cm^2 was used, allocating inside an anode of 2 cm^2 of iron foil. A magnetic stirrer was placed inside the batch cell. The temperature was maintained at 25 °C.

Using an Amel Electrochemistry Galvanostat (Model 549), (Italy), a constant current was applied to the electrodes for 30 min. The iron anode was oxidized, producing iron ions, and while in the cathode, the water was reduced to hydroxyl ions. Therefore, in the solution, cobalt, nickel, iron and hydroxyl ions reacted and formed $Fe_y^{2+}M_x^{2+}Fe_{3-x-y}^{3+}O_4$. After this time, the solution was placed over a magnet to collect the product, which was thoroughly washed with deionized water and dried in vacuum. The supernatants were analysed with inductively coupled plasma optical emission spectroscopy (ICP-OES) to obtain the removal rate (%).

The effectiveness in removing these metals was evaluated using different concentrations of metallic ions (Co^{2+}, Ni^{2+} and a mixture of $Co^{2+} + Ni^{2+}$) in a concentration range of 50–400 ppm. Furthermore, the influence of the current density applied on the removal efficiency was studied.

2.2.2. Flow reactor

In this reactor, 8 plates (100 mm × 45 mm) were used as electrodes and were machined out of low carbon steel sheets of 1 mm thickness and 99.8% wt iron purity and arranged in a parallel monopolar configuration. A small 5 mm section protruded from the edge of each of the electrodes to use as an electrical connection and a 10 mm separation was kept between electrodes in all chambers. Two-litre solutions of 100 ppm M^{2+} and 40 mM NaCl were used as simulated pollutant solutions, the cell's total volume was 460 mL. Direct current of 0.7 A was supplied using a Dosban Industrial AFX3333C DC (Spain) power supply and a

multimeter connected in series to confirm the total current value. The solution continuously flowed using a Heidolph Pumpdrive 5201 (Germany) peristaltic pump operating at 30 mL/min [26]. Aliquots of the supernatant were analysed with an Optima 2100 DV PerkinElmer (ICP-OES) equipment. The magnetically collected sample at the end of the experiment was washed several times with distilled water and the Co and Ni content were measured by ICP-OES. A scheme of the process is shown in Fig. 1.

2.3. Characterization techniques

Transmission electron microscopy (TEM) samples were prepared by dispersing a minimal amount of nanoparticles ($\approx$1 mg) in an aqueous solution, placing a single drop onto a copper grid coated with a carbon film, and letting it dry. The TEM analysis was then carried out in a JEOL JEM 1010 operating at an acceleration voltage of 100 kV. STEM-HAADF (scanning-transmission imaging with a high-angle annular dark field detector) results were obtained using a Tecnai F30 (FEI) electron microscope operated at 300 kV. Chemical analysis of the nanoparticles was performed by energy dispersive X-ray microanalysis (EDX).

Phase identification and crystal structure of the magnetic materials were analysed by X-ray diffraction (XRD) performed in a Philips X'Pert Pro Theta/theta diffractometer CuKα radiation (λ = 1.5406 Å) with a secondary graphite monochromator that discriminates the fluorescence. The patterns were collected within 10° and 80° in 2θ, with an angular increment of 0.04° and incremental time of 4 s.

The field dependent magnetization curves were measured at room temperature by applying a maximum magnetic field of 5 T, on dried powder samples using a vibrating sample magnetometer (VSM; MLVSM9 MagLab 9 T, Oxford Instrument). From the magnetization curves, the saturation magnetization (M_s), the remanence (M_r) and the coercivity (H_c) were calculated.

3. Results and discussion

3.1. Batch experiments

3.1.1. Pollutant concentration and current density effect

Fig. 2a depicts the Ni and Co removal efficiency determined from the ICP-OES quantification of the remaining metal ion concentration in the supernatant after 30 min of the experiment. A clear tendency is observed; when the initial concentration increases, the efficiency decreases for both pollutants. For an initial concentration of 50 ppm, the elimination of Co and Ni ions is close to 100%, with values of 98% and 95%, respectively. When the concentration increases, the removal efficiency of Co ions drastically decreases to 78% when the initial concentration is 200 ppm. Nevertheless, in the case of Ni ions, this decrease does not occur, maintaining a stable efficiency value of approximately 95% over the entire range of studied concentrations. This behaviour can be explained by the smaller atomic ratio of Ni ions compared to cobalt ions.

The magnetic recovery of the resulting samples represents an important advantage of the methodology. Nevertheless, when working in the presence of 200 ppm pollutant, either nickel or cobalt, the magnetic recovery of the obtained product is slow. To understand this phenomenon, TEM analysis of these samples was performed, observing that in these two cases, we obtained laminar structures typical of oxyhydroxides such as lepidocrocite, ϒ-FeOOH (Fig. 2b and c).

To recover as much pollutant as possible and produce ferrites with good magnetic properties, the current density was doubled from 50 mA/cm^2 to 100 mA/cm^2, starting at 200 ppm. A significant increase, mainly in cobalt recovery, was observed under such conditions (Fig. 2a, stars). In contrast, the nickel improvement removal efficiency was smaller under these conditions. The current density increase favoured the oxidation rate of the iron foil and the delivery of Fe ions throughout the solution; for that reason, the formation of a ferrite structure is favoured.
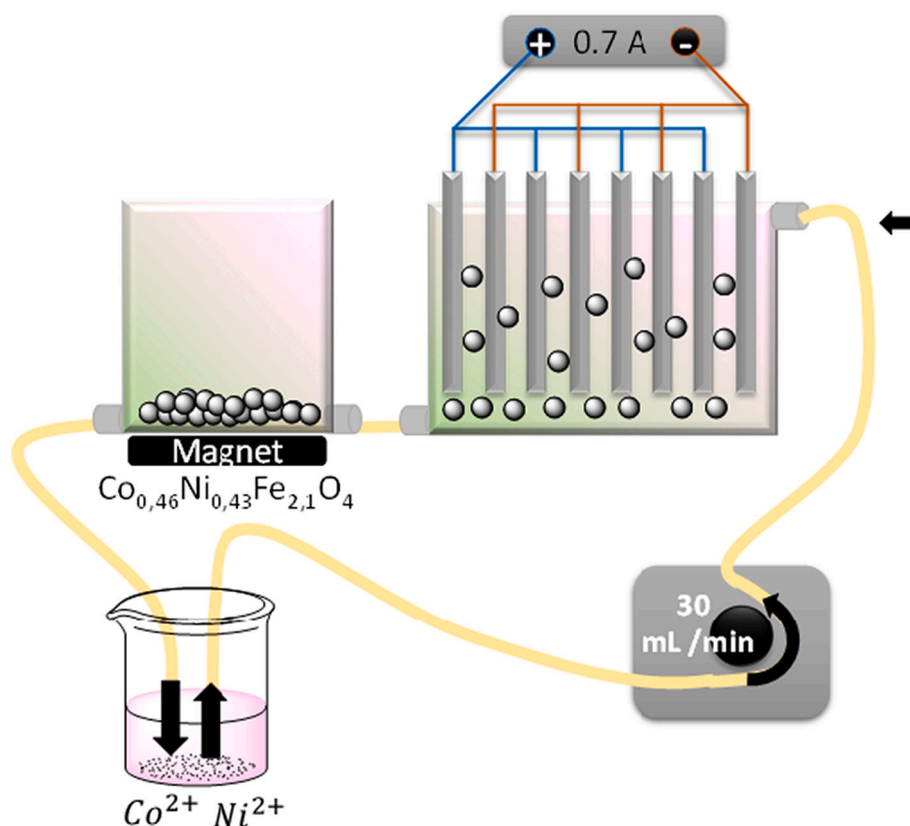
Fig. 1. Scheme of the finished prototype flow cell reactor.

The TEM images of the obtained ferrites showed polydisperse nanoparticles with quasi-spherical shapes, with an average size of 30(8) nm for the cobalt sample and 26(9) for the nickel sample (Fig. 2d and e). These samples were easily removed with a magnet. Although an increase in the current density showed a marked improvement in the recovery efficiency and promotes the formation of mixed ferrites nanoparticles, it is a limiting parameter because a high current density can cause rapid degradation of the iron electrode and the appearance of metallic iron in the ferrite structure or solution.

The compounds obtained under 100 ppm and a 50 mA/cm^2 current density showed a typical spinel crystal structure, whose reflections can be attributed to the Fd-3m (227) space group (Fig. 3a). The nanoparticles obtained showed flower-like shapes with average nanoparticle sizes of 30(10) nm and 27(7) nm for cobalt ferrite and nickel ferrite, respectively (Fig. 3b, c, d).

The two samples described above, obtained under optimal conditions, had enough strong magnetic properties to be recovered by a magnet. To confirm this behaviour, the hysteresis cycles were measured at room temperature (Fig. 4). The collected magnetic parameters are summarized in Table 1. The presence of cobalt atoms in the spinel structure results in the aperture of the hysteresis cycle with a coercivity (H_c) of 225 Oe. On the other hand, nickel ferrite results in a narrower cycle, indicating that the material is magnetically softer with a coercivity equal to 59 Oe at room temperature. The remanences of the cobalt and nickel samples were 12 emu/g and 6 emu/g, respectively. The higher remanence agrees with cobalt ferrite formation, given that for similar sizes, iron oxide and nickel ferrite usually presents lower remanence values.

The cobalt, nickel, and iron contents in the two ferrites were quantified by ICP-OES to estimate the stoichiometry of the compounds formed. The following values were obtained: $Co_{0.20}Fe_{2.80}O_4$ and $Ni_{0.44}Fe_{2.56}O_4$. The M_r/M_s squareness ratio showed in Table 1 for cobalt ferrite sample agrees with some values reported for cobalt ferrite

nanoparticles with same stoichiometry and similar sizes [27]. In addition, the M_s is lower than the bulk value and close to other values reported with the same inversion degree and similar sizes [27]. The higher Ni concentration in the nickel sample in comparison with the cobalt sample was consistent with the higher removal percentage obtained with Ni pollutant, Fig. 2a. The ICP-OES analysis provided useful evidence about the presence of cations in the bulk material; however, it did not provide information about the location of the different atoms in the particles. To analyse this, STEM-HAADF coupled with EDX was used to measure the presence of Co, Ni, and Fe along the isolated particles (Fig. 5). Results indicated a homogenous distribution of the Ni and Co within the particles. Also, all the particles tested showed the presence of Fe, O, and the corresponding metal, discarding the formation of other type of compositions being formed.

3.1.2. Temperature effect in the removal efficiency

Another key factor which affects the oxidation rate of the iron foil and the removal efficiency is the temperature of the solution. Higher temperatures imply higher oxidation rates and a greater concentration of Fe to be recombined with Co or Ni ions to form the ferrite samples. Preliminary results shown that if the temperature is increased from 25 °C up to 60 °C for the conditions 200Co - i50, the percentage removal increased from 78% up to 89%, the XRD pattern and the TEM micrography are represented in Fig. 6. XRD analysis reveals a cleaner pattern compared with the 25 °C sample (Fig. 6a), with the main presence of cubic reflexions attributed to ferrite sample, but also an important presence of cubic iron phase (Space group: Im-3m (229) – JCPDS: 01-087-0721), formed either by the degradation of the iron foil or by the reduction of iron ions in cathode, by the temperature effect. In contrast the XRD obtained for the sample of the experience conducted at 25 °C shown the presence of iron oxyhydroxides (JCPDS: 01-070-0713), but also the presence of cobalt ferrite in low percentage is not discarded. The NPs formed at 60 °C are bigger, with a mean diameter of 38(10) nm.
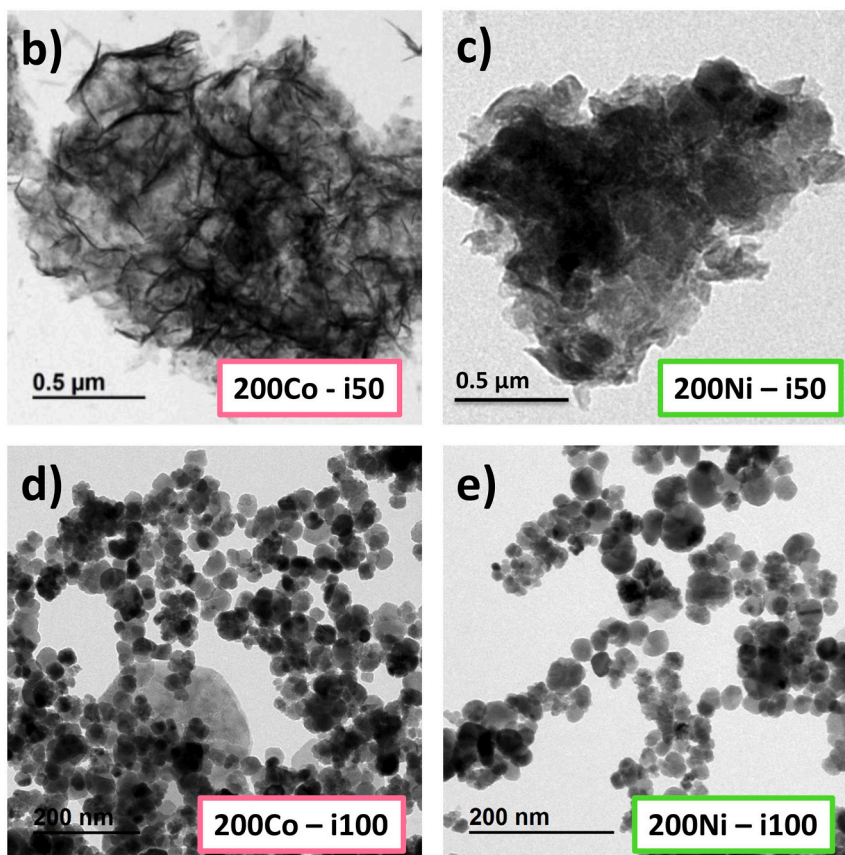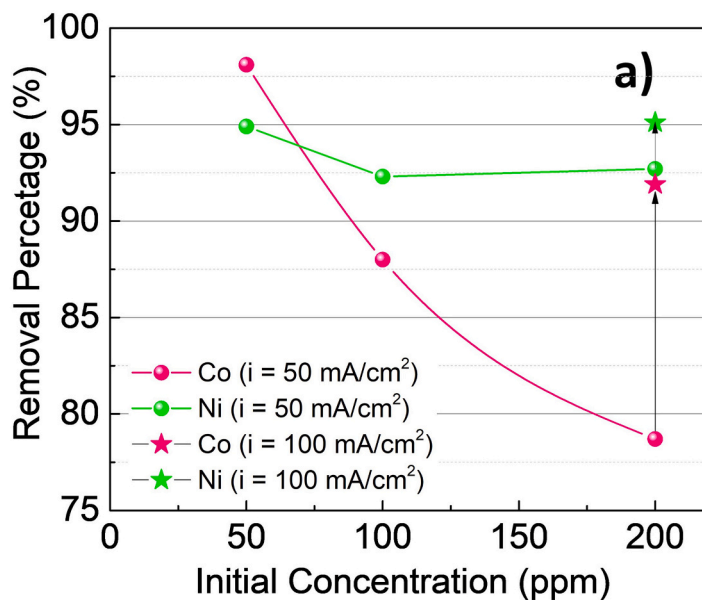
Fig. 2. a) Removal efficiency of Cobalt and Nickel from contaminated solutions as a function of the initial concentration (50–200 ppm) and current density applied (50–100 mA/cm^2). In an experiment time of 30 min. b) and c) TEM images of samples obtained with 200 ppm of initial solution and $i = 50$ mA/cm^2, of cobalt and nickel respectively. d) and e) TEM images of samples obtained with 200 ppm of initial solution and $i = 100$ mA/cm^2, of cobalt and nickel, respectively.

### 3.1.3. Batch experiment in mixed pollutant solution

After testing the recovery efficiencies of both Co and Ni elements individually, the following stage consisted of putting both ions into the same vessel and evaluating the effectiveness of the process. Here, the current density and temperature were fixed at 50 mA/cm^2 and 25 °C, respectively, to compare with the results obtained above and avoid the degradation of iron metal. The total pollutant concentrations were 100, 200, and 400 ppm (divided between Co and Ni at 50% each). For

comparison, the removal efficiency obtained starting with 100 and 200 ppm of only Co and Ni is also represented in Fig. 7.

If 100 ppm contaminant was used in the solution, namely, 50 ppm Ni and 50 ppm cobalt, the recoveries of both were favoured, being 93 and 91%, respectively (Fig. 7). In contrast, in Fig. 2a, we showed a slightly lower recovery when the contaminant was exclusively 100 ppm Co or Ni, with values of 88% and 92%, respectively. The same trend was observed with 100 ppm Ni + 100 ppm Co. In this case, the improvement
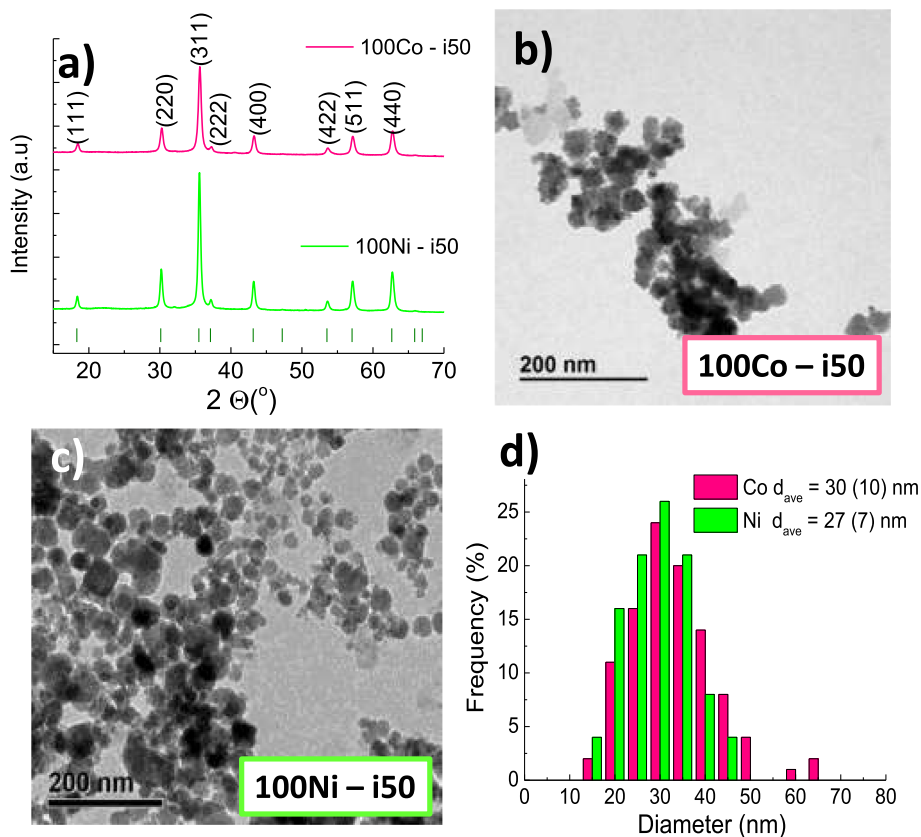
Fig. 3. a) XRD diffractogram of the compounds obtained starting with 100 ppm of Co or 100 ppm of Ni and current density applied of 50 mA/cm². (Bragg positions labeled of space group 227). JCPDS cards for cobalt ferrite (00-003-0864) and nickel ferrite samples (01-087-2336). b) and c) TEM micrograph of samples obtained starting with 100 ppm of Co or 100 ppm of Ni in solution, respectively. d) Histogram analysis of particle size referred to samples b) and c).
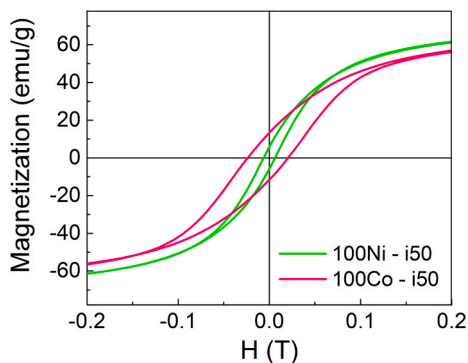
Fig. 4. M-H loops obtained with a maximum magnetic field of 5 T of the two compounds obtained with 100 ppm of Co and 100 ppm of Ni with $i = 50$ mA/cm².

Table 1
Magnetic parameters obtained from the analysis of the M-H loops at 298 K.

|	H_c (Oe)	M_r (emu/g)	M_s (emu/g)	M_r/M_s	Formula ICP	D_{TEM} (nm)
100Ni – i50	59	6	75(1)	0.08	$Ni_{0.44}Fe_{2.56}O_4$	27(7)
100Co – i50	225	12	73(2)	0.16	$Co_{0.20}Fe_{2.80}O_4$	30 (10)
100Co – 100Ni – i50	381	15	59(1)	0.25	$Co_{0.32}Ni_{0.25}Fe_{2.43}O_4$	26(9)

in cobalt removal efficiency reached 87% (78% starting with 200 ppm cobalt), while the removal efficiency of Ni slightly decreased up to 89% (93% starting with 200 ppm nickel). The combination of both pollutants seems to improve the total pollutant weight recovered. This finding was previously reported with an adsorbent prepared from an electronic waste-based material [28], and sodium activated bentonite [29], where the adsorption of Co and Ni in a binary wastewater metal system is enhanced in comparison with the single metal system.

It is important to highlight that the material formed with the mixture of both pollutants up to 200 ppm in total results in the formation of almost spherical nanoparticles (Fig. 8a), with an average size of 26(9) nm. This result was not observed in Fig. 2b and c, when 200 ppm was composed exclusively of either nickel or cobalt. The XRD presented also in Fig. 6, reveals a mixture of different phases for Co200-i50 sample, this behaviour was also observed for Ni200-i50 sample (data not shown). In contrast, in the sample containing both pollutants (100Co–100Ni – i50), the diffractogram showed a purely spinel-type structure, typical of ferrites, and no traces of other iron oxide phases, Fig. 8b.

The room temperature hysteresis loops confirmed the presence of cobalt within the structure, and the magnetic coercivity was approximately 381 Oe, (Fig. 8c) higher than the H_c obtained in the cobalt compound, 100Co – i50 (Fig. 4), which was 225 Oe at room temperature, Table 1. This evidence confirmed the presence of cobalt within the structure, which was also corroborated by ICP-OES analysis of the powder. The stoichiometric formula obtained was $Co_{0.32}Ni_{0.25}Fe_{2.43}O_4$. The higher cobalt content observed in the ICP-OES analysis agreed with the higher removal percentage observed when working with the pollutant mixture and with greater values of H_c of this sample in comparison with the cobalt ferrite sample, 100Co – i50. A lower content of nickel within the structure was observed, which agrees with the decrease in percentage efficiency in comparison with the experiment
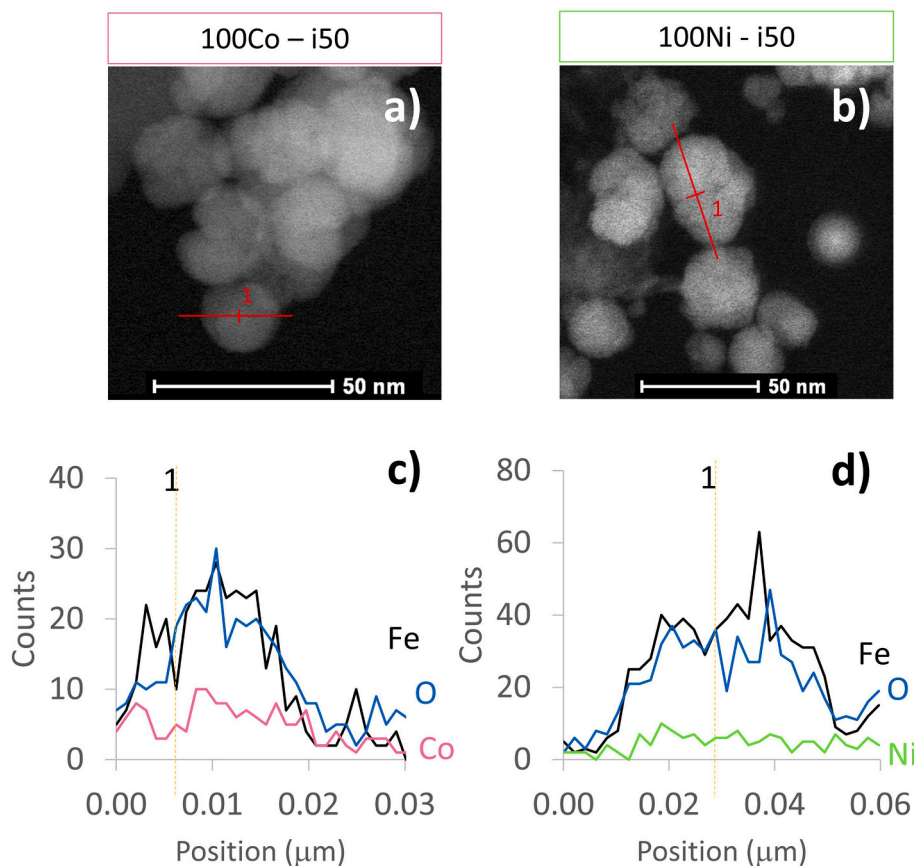
Fig. 5. STEM-HAADF images (top) and EDX analysis (bottom) for samples obtained with 100 ppm of Co (a and c) and Ni ions (b and d) and $i = 50$ mA/cm². The red line marked in the upper images indicates the position in which the EDX analysis has been made, being the position in number 1 from the EDX plot the same as marked in the images. (For interpretation of the references to color in this figure legend, the reader is referred to the web version of this article.)
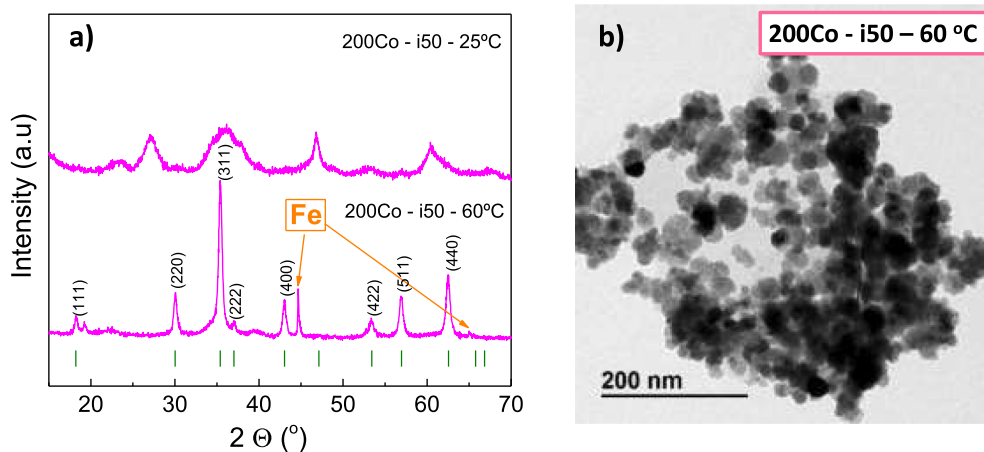
Fig. 6. a) XRD of samples obtained starting with 200 ppm of Co and $i = 50$ mA/cm² at 25 °C and 60 °C. (Bragg positions labeled of space group 227). JCPDS cards for cobalt ferrite (00-003-0864). b) TEM micrograph of the sample 200Co – i50–60 °C.

using only 100 ppm of nickel.

If we increased the pollutant concentration up to 400 ppm, both ions were at a concentration of 200 ppm there was a sharp decrease in efficiency, and the compound formed had a non-nanoparticulate morphology, but in the form of needles, images are not shown. Slightly magnetic material was obtained. In this sense, the reason for this reduced elimination might be the poor iron ions concentration released into the solution in comparison with the Co and Ni content. In this regard, an increment of current density applied to the iron foil promotes

an increase in the concentration of released ions and an improved removal percentage, as demonstrated in Fig. 2a, when increasing the current density from 50 mA/cm² to 100 mAcm² resulted in a significant increase in the % of cobalt removed.

Considering these results, there was a limitation in the maximum concentration that could be removed with this methodology and with the current density applied. An aqueous simulated pollutant solution with 100 ppm Co and Ni seemed to be the upper limit because under such conditions, the formed nanoparticles had enough strong magnetic
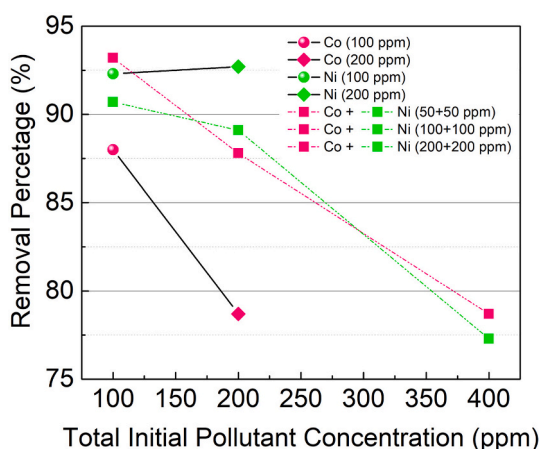
Fig. 7. Removal percentage obtained with different mixtures of (Ni + Co) pollutant concentrations, divided between Co and Ni at 50% each, filled squares. For comparison, the removal efficiencies of samples obtained with only Ni or Co as pollutant agent is also represented.

properties to be recovered with a magnet, they had a crystalized structure, and in addition, the removal efficiency was approximately 90% for both pollutants.

These results indicate that we have found an easy methodology to remove cobalt ions, nickel ions, and a mixture of both, producing materials with good properties and suitability for use in different applications, including fenton degradation process [30,31] and adsorption

pollutant removal [32,33]. To go one step further, the electrochemical module was modified to perform contaminant removal in a continuous way.

3.2. Flow reactor cell

Using the flow reactor in Fig. 1, we tested the removal of pollutants using concentrations of Co and Ni ions of 100 ppm each in a 2 L vessel, applying a current of 0.7 A over 1 h. The removal efficiency through this process was approximately 91% and 96% for cobalt and nickel, respectively. The obtained nanoparticles presented a ferrite structure with no additional phases, and only those peaks corresponding to a spinel with cobalt and nickel atoms substituting Fe^{2+} atoms in the magnetite structure were found in the XRD diffractogram (Fig. 9a). The formula of the material obtained was $Co_{0.46}Ni_{0.43}Fe_{2.1}O_4$. The particles presented a spherical morphology with a diameter size of approximately 25 nm and a standard deviation of 10 nm (Fig. 9b). By using this continuous flow system, it was possible to remove both ions from 2 L of pollutant solution with good removal efficiency and perform the process in a continuous way. This continuous procedure significantly improved the removal of heavy metals, opening the way for further studies.

4. Conclusions

This work proposes a new methodology for the recovery of cobalt and nickel ions independently or in the same solution together with the formation of cobalt and nickel or mixed ferrites whose morphological, structural, and magnetic characteristics may vary with experimental conditions. When ion recovery is carried out at current densities of 50
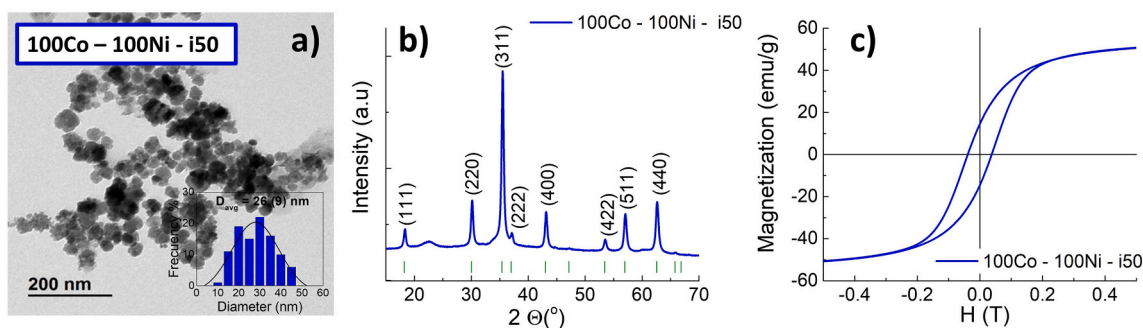

Fig. 8. a) TEM micrograph of sample obtained starting with a mixture of pollutant, 100 ppm Ni + 100 ppm Co in solution and $i = 50$ mA/cm², (100Co - 100Ni - i50 sample). Inset, size distribution of the nanoparticles. b) XRD of the 100Co - 100Ni - i50 sample. (Bragg positions of the space group 227 are labeled). c) M-H loops obtained with a maximum magnetic field of 5 T for the sample 100Co - 100Ni - i50.
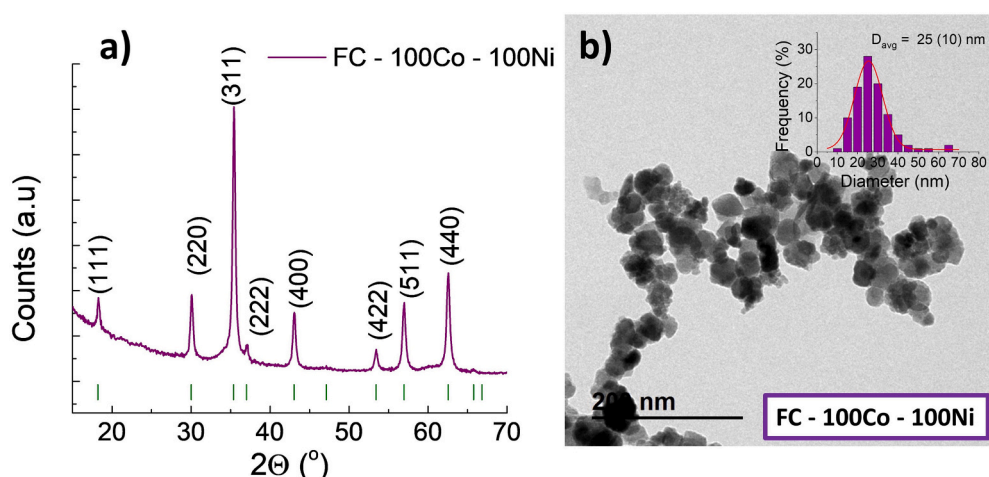

Fig. 9. a) XRD difractogram of FC – 100Co – 100Ni. (Bragg positions of the space group 227 are labeled). b) TEM image and histogram analysis of diameter size.

mA/cm^2, the recovery efficiency is close to 100% for concentrations less than 100 ppm, and the particles obtained are quasi-spherical with sizes on the order of 27 nm, with properties of a ferromagnetic material. Increasing the concentration to 200 ppm showed a clear decrease in recovery efficiency. Increasing the current density to $100\,mA/cm^2$ or the temperature up to $60\,°C$ produces the appearance of metallic iron in the obtained material, but also increased the removal efficiencies. Therefore, we can conclude that under the experimental conditions of this work, total recovery is not possible for ion concentrations greater than 100 ppm. The most important conclusion of this work is the possibility of recovering high amounts of cobalt and nickel ions in a continuous flow cell, which allows recovery in much larger volumes of contaminants.

Declaration of competing interest

The authors declare that they have no known competing financial interests or personal relationships that could have appeared to influence the work reported in this paper.

References

[1] L. Petrick, Y. Dubowski, S. Klas, O. Lahav, Stable incorporation of Co^{2+} into ferrite structure at ambient temperature: effect of operational parameters, Water Air Soil Pollut. 190 (2008) 245–257, https://doi.org/10.1007/s11270-007-9597-4.

[2] S. Rengaraj, K.-H. Yeon, S.-Y. Kang, J.-U. Lee, K.-W. Kim, S.-H. Moon, Studies on adsorptive removal of Co(II), Cr(III) and Ni(II) by IRN77 cation-exchange resin, J. Hazard. Mater. 92 (2002) 185–198. http://www.sciencedirect.com/science/article/pii/S0304389402000183.

[3] M. Jouyandeh, M.R. Ganjali, J.A. Ali, M. Aghazadeh, F.J. Stadler, M.R. Saeb, Curing epoxy with electrochemically synthesized $Co_xFe_{3-x}O_4$ magnetic nanoparticles, Prog. Org. Coat. 137 (2019), 105252. http://www.sciencedirect.com/science/article/pii/S0300944019307763.

[4] L. Tofan, C. Teodosiu, C. Paduraru, R. Wenkert, Cobalt (II) removal from aqueous solutions by natural hemp fibers: batch and fixed-bed column studies, Appl. Surf. Sci. 285 (2013) 33–39. http://www.sciencedirect.com/science/article/pii/S0169433213012804.

[5] A.I. Ivanets, V. Srivastava, M.Y. Roshchina, M. Sillanpää, V.G. Prozorovich, V. V. Pankov, Magnesium ferrite nanoparticles as a magnetic sorbent for the removal of Mn^{2+}, Co^{2+}, Ni^{2+} and Cu^{2+} from aqueous solution, Ceram. Int. 44 (2018) 9097–9104. http://www.sciencedirect.com/science/article/pii/S0272884218304140.

[6] L.J. Martínez, A. Muñoz-Bonilla, E. Mazario, F.J. Recio, F.J. Palomares, P. Herrasti, Adsorption of chromium(VI) onto electrochemically obtained magnetite nanoparticles, Int. J. Environ. Sci. Technol 12 (2015), 4017–4024–2015 v.12 no.12.

[7] A. Gallo-Cordova, M. del P. Morales, E. Mazarío, Effect of the surface charge on the adsorption capacity of chromium(VI) of Iron oxide magnetic nanoparticles prepared by microwave-assisted synthesis, Water. 11 (2019).

[8] X.S. Song, S.F. Wang, J.Y. Lu, Removal of chromium and nickel ions from synthetic solution by the ferrite process, Adv. Mater. Res. 113–116 (2010) 2251–2254. https://www.scientific.net/AMR.113-116.2251.

[9] J.H. Cheong, K.J. Lee, Removal of Co^{2+} ions from aqueous solution by ferrite process, Sep. Sci. Technol. 31 (1996) 1137–1160, https://doi.org/10.1080/01496399608001339.

[10] G. Huang, P. Dou, Z. Zhang, J. Yan, Removal of cobalt from liquid radioactive waste by in situ electrochemical synthesis of ferrite, J. Radioanal. Nucl. Chem. 316 (2018) 61–70, https://doi.org/10.1007/s10967-018-5766-8.

[11] Y. Xue, Y. Wang, Green electrochemical redox mediation for valuable metal extraction and recycling from industrial waste, Green Chem. 22 (2020) 6288–6309, https://doi.org/10.1039/D0GC02028A.

[12] B. Sahoo, K.S.P. Devi, S. Dutta, T.K. Maiti, P. Pramanik, D. Dhara, Biocompatible mesoporous silica-coated superparamagnetic manganese ferrite nanoparticles for targeted drug delivery and MR imaging applications, J. Colloid Interface Sci. 431 (2014) 31–41. http://www.sciencedirect.com/science/article/pii/S002197971400383X.

[13] E. Naderi, M. Aghajanzadeh, M. Zamani, A. Sharafi, M. Naseri, H. Danafar, The effect of calcination temperature on the anticancer activity of $CaFe_2O_4$@PVA nanocarriers: photodynamic therapy and drug delivery study, J. Inorg. Organomet. Polym. Mater. (2020), https://doi.org/10.1007/s10904-020-01653-z.

[14] T. Zargar, A. Kermanpur, Effects of hydrothermal process parameters on the physical, magnetic and thermal properties of $Zn_{0.3}Fe_{2.7}O_4$ nanoparticles for magnetic hyperthermia applications, Ceram. Int. 43 (2017) 5794–5804. http://www.sciencedirect.com/science/article/pii/S0272884217301499.

[15] J. Jaime-González, E. Mazario, N. Menendez, J. Sanchez-Marcos, A. Muñoz-Bonilla, P. Herrasti, Comparison of ferrite nanoparticles obtained electrochemically for catalytical reduction of hydrogen peroxide, J. Solid State Electrochem. 20 (2016) 1191–1198.

[16] R. Galindo, E. Mazario, S. Gutiérrez, M.P. Morales, P. Herrasti, Electrochemical synthesis of $NiFe_2O_4$ nanoparticles: characterization and their catalytic applications, J. Alloys Compd. 536 (2012).

[17] A. Hassani, M. Karaca, S. Karaca, A. Khataee, Ö. Açışlı, B. Yılmaz, Preparation of magnetite nanoparticles by high-energy planetary ball mill and its application for ciprofloxacin degradation through heterogeneous Fenton process, J. Environ. Manag. 211 (2018) 53–62. http://www.sciencedirect.com/science/article/pii/S0301479718300148.

[18] L. Zhao, Z.-R. Lin, X. Ma, Y.-H. Dong, Catalytic activity of different iron oxides: insight from pollutant degradation and hydroxyl radical formation in heterogeneous Fenton-like systems, Chem. Eng. J. 352 (2018) 343–351. http://www.sciencedirect.com/science/article/pii/S1385894718312683.

[19] L.P. Lingamdinne, Y.-Y. Chang, J.-K. Yang, J. Singh, E.-H. Choi, M. Shiratani, J. R. Koduru, P. Attri, Biogenic reductive preparation of magnetic inverse spinel iron oxide nanoparticles for the adsorption removal of heavy metals, Chem. Eng. J. 307 (2017) 74–84. http://www.sciencedirect.com/science/article/pii/S138589471631141X.

[20] F. Liu, K. Zhou, Q. Chen, A. Wang, W. Chen, Application of magnetic ferrite nanoparticles for removal of Cu(II) from copper-ammonia wastewater, J. Alloys Compd. 773 (2019) 140–149. http://www.sciencedirect.com/science/article/pii/S092583881833487X.

[21] A.S. Helal, E. Mazario, A. Mayoral, P. Decorse, R. Losno, C. Lion, S. Ammar, M. Hémadi, Highly efficient and selective extraction of uranium from aqueous solution using a magnetic device: succinyl-β-cyclodextrin-APTES@maghemite nanoparticles, Environ. Sci. Nano. 5 (2018) 158–168, https://doi.org/10.1039/C7EN00902J.

[22] N. Tran, A. Mir, D. Mallik, A. Sinha, S. Nayar, T.J. Webster, Bactericidal effect of iron oxide nanoparticles on Staphylococcus aureus, Int. J. Nanomedicine 5 (2010) 277–283. https://www.scopus.com/inward/record.uri?eid=2-s2.0-77951199256&partnerID=40&md5=e0b94748b2c72592d4d867bee3ce1268.

[23] S. Zhan, D. Zhu, S. Ma, W. Yu, Y. Jia, Y. Li, H. Yu, Z. Shen, Highly efficient removal of pathogenic Bacteria with magnetic graphene composite, ACS Appl. Mater. Interfaces 7 (2015) 4290–4298, https://doi.org/10.1021/am508682s.

[24] M. Rivero, A. del Campo, Á. Mayoral, E. Mazario, J. Sánchez-Marcos, A. Muñoz-Bonilla, Synthesis and structural characterization of $Zn_xFe_{3-x}O_4$ ferrite nanoparticles obtained by an electrochemical method, RSC Adv. 6 (2016) 40067–40076, https://doi.org/10.1039/C6RA04145K.

[25] Á. Gallo-Cordova, A. Espinosa, A. Serrano, L. Gutiérrez, N. Menéndez, M. del Puerto Morales, E. Mazarío, New insights into the structural analysis of maghemite and (MFe_2O_4, M⎯Co, Zn) ferrite nanoparticles synthesized by a microwave-assisted polyol process, Mater. Chem. Front. 4 (2020) 3063–3073, https://doi.org/10.1039/D0QM00460J.

[26] I. Lozano, C. López, N. Menendez, N. Casillas, P. Herrasti, Design, construction and evaluation of a 3D printed electrochemical flow cell for the synthesis of magnetite nanoparticles, J. Electrochem. Soc. 165 (2018) H688–H697.

[27] H. Sharifi Dehsari, K. Asadi, Impact of stoichiometry and size on the magnetic properties of cobalt ferrite nanoparticles, J. Phys. Chem. C. 122 (2018) 29106–29121, https://doi.org/10.1021/acs.jpcc.8b09276.

[28] P. Hadi, J. Barford, G. McKay, Synergistic effect in the simultaneous removal of binary cobalt–nickel heavy metals from effluents by a novel e-waste-derived material, Chem. Eng. J. 228 (2013) 140–146. http://www.sciencedirect.com/science/article/pii/S1385894713005846.

[29] S. Triantafyllou, E. Christodoulou, P. Neou-Syngouna, Removal of nickel and cobalt from aqueous solutions by Na-activated bentonite, Clay Clay Miner. 47 (1999) 567–572. https://www.scopus.com/inward/record.uri?eid=2-s2.0-0033208521&doi=10.1346%2FCCMN.1999.0470503&partnerID=40&md5=7bda17b6aa84779d0e18bd5164e497b7.

[30] F.L. Rivera, F.J. Recio, F.J. Palomares, J. Sánchez-Marcos, N. Menéndez, E. Mazarío, P. Herrasti, Fenton-like degradation enhancement of methylene blue dye with magnetic heating induction, J. Electroanal. Chem. 879 (2020), 114773, https://doi.org/10.1016/j.jelechem.2020.114773.

[31] S. Rahim Pouran, A.A. Abdul Raman, W.M.A. Wan Daud, Review on the application of modified iron oxides as heterogeneous catalysts in Fenton reactions, J. Clean. Prod. 64 (2014) 24–35, https://doi.org/10.1016/j.jclepro.2013.09.013.

[32] E. Mazarío, J. Stemper, A.S. Helal, A. Mayoral, P. Decorse, R. Losno, C. Lion, S. Ammar, T.L. Gall, M. Hémadi, New Iron oxide nanoparticles catechol-grafted with Bis(amidoxime)s for uranium(VI) depletion of aqueous solution, J. Nanosci. Nanotechnol. 19 (2019), https://doi.org/10.1166/jnn.2019.16804.

[33] F.L. Rivera, F.J. Palomares, P. Herrasti, E. Mazario, Improvement in heavy metal removal from wastewater using an external magnetic inductor, Nanomaterials. 9 (2019), https://doi.org/10.3390/nano9111508.